

Contents lists available at ScienceDirect

Environmental Pollution and Management

journal homepage: www.keaipublishing.com/en/journals/epm



Dual-functional CuO/ZrO₂/Al₂O₃ nanocomposite with tailored p–n heterojunction interfaces for enhanced dye degradation and antimicrobial efficiency



Vivekraj Nagaraju^a, Jagadish Krishnegowda^b, Lingegowda Nagarakere Shivalingaiah^c, Thriveni Muttegere Karigiregowda^d, Kumara Manikyanahally Narasigowda^a,*

- ^a Department of Chemistry, Yuvaraja's College, University of Mysore, Mysuru, Karnataka 570005, India
- b Department of Chemistry (PG), Sarada Vilas College, University of Mysore, Mysuru, Karnataka 570006, India
- ^c Department of Chemistry, Vidhya Vardhaka College of Engineering, Mysuru, Karnataka, India
- d Department of Chemistry, Maharaja Institute of Technology, Mysuru, Karnataka, India

ARTICLE INFO

Keywords: CuO/ZrO₂/Al₂O₃ Nanocomposite Electrochemical synthesis Photocatalysis Biocompatibility

ABSTRACT

A highly efficient $CuO/ZrO_2/Al_2O_3$ ternary nanocomposite was synthesized using a green and cost-effective electrochemical method. The crystallinity, morphology, elemental composition, surface adsorption (BET), optical, catalytic and biological properties of the nanocomposite was systematically characterized using advanced analytical techniques. XRD analysis confirmed the presence of distinct peaks corresponding to CuO, ZrO_2 , and Al_2O_3 , indicating the successful formation of a visible-light-active catalyst. SEM images revealed strong interfacial interactions between CuO and ZrO_2 integrated within the porous, high-surface-area structure of Al_2O_3 , UV-Visible and DRS analysis determined the band gap energy to be $2.5\,eV$. The nanocomposite demonstrated excellent photocatalytic efficiency in degrading Indigo Carmine (IC) dye, achieving up to 95 % removal. The high surface area of Al_2O_3 (195 m^2/g) facilitated dye adsorption, while the CuO- ZrO_2 heterojunction enhanced charge separation: sunlight-excited electrons from p-type CuO were transferred to n-type CuO reducing recombination. Additionally, the nanocomposite exhibited significant antimicrobial activity against various bacterial and fungal strains, outperforming standard references. The novelty of this work lies in the green electrochemical synthesis of a $CuO/ZrO_2/Al_2O_3$ ternary heterojunction photocatalyst that uniquely combines high surface area, efficient charge separation, and visible-light activity, enabling dual photocatalytic and antimicrobial functionality.

1. Introduction

The science of nanotechnology involves controlling matter at the nanoscale, a dimension that typically ranges from 1 to 100 nanometers [1–3]. This entails employing atoms and molecules to design, create and operate systems, devices and structures [4–6]. Materials with unique qualities can be engineered at this scale, offering broad applications in electronics, healthcare, and energy. [7,8]. Compared to conventional materials, they offer improved performance and functionality because of their capacity to mix the characteristics of many materials at the nanoscale [9–11]. They are appropriate for a variety of applications because they have benefits in areas including strength, durability, thermal stability and barrier qualities [12–15].

Compounds known as metal oxides are created when a metal and oxygen combine (Al_2O_3 , ZrO_2 , NiO, Fe_3O_4 , ZnO, CuO, and TiO_2) [16,17]. Applications for them are numerous and varied, ranging from electronics to environmental cleanup and catalysis [18]. Their significance stems from a high surface area, semiconducting ability, and involvement in redox and acid-base interactions [19,20]. Because they are more versatile and have better qualities than their individual components, nanocomposite metal oxides are significant [21]. Applications for them are numerous and include environmental remediation, energy storage, sensors, and catalysis [22,23]. This customization capability makes them a significant area of research in materials science and nanotechnology. [24,25].

Due to their unique properties, copper oxide (CuO) nanoparticles and nanocomposites have attracted global interest for use in energy and

Peer review under the responsibility of Editorial Board of Environmental Pollution and Management.

E-mail address: kumaramanikya73@gmail.com (K.M. Narasigowda).

https://doi.org/10.1016/j.epm.2025.10.002

^{*} Corresponding author.

environmental applications [26]. In this article, several methods for creating CuO nanoparticles and their possible uses are covered [27]. In-depth research is done on both conventional and environmentally friendly synthesis methods as well as how reaction circumstances affect the produced nanoparticles [28,29]. Zirconia of biomedical grade shows possible mechanical properties of oxide ceramics [30]. This study assessed the dispersion stability of ZrO2 nanofluids over time by using anionic, cationic, and non-ionic surfactants for stabilization. [31]. Up to 1200 °C, Al₂O₃ stability was increased while the sintering of that phase was improved [32]. Aluminum nanoparticles are especially vulnerable to severe oxidation during storage before use because of their small diameters [33]. Nanomaterials are having an impact on pharmacological and biological applications [34–36].

As nanocomposites, these materials benefit from nanoscale effects, large surface-to-volume ratio, abundant active sites, and quantum confinement that accelerate interfacial charge transfer and improve light harvesting capability. In photocatalytic degradation of organic pollutants, the nanocomposite architecture provides a dual advantage: (i) efficient generation of reactive oxygen species (ROS) such as $O_2^{\bullet,-}$ and 'OH through multi-path electron transitions, and (ii) enhanced adsorption of dye molecules on the catalyst surface due to increased porosity and surface energy.

Under optimal conditions, transition-metal-decorated Fe₃O₄ catalysts achieved about 97 % degradation of Carbol Fuchsin dye, while doped Fe₂O₃ systems reached complete (100%) removal under specific conditions [37]. Incorporation of Fe³⁺ into ZnO nanomaterials enhanced charge separation, enabling efficient methylene blue degradation and improved ethanol gas sensing [38]. Similarly, transition-metal-doped Bi₂O₃ nanophotocatalysts exhibited superior light utilization and dye removal efficiency [39]. Furthermore, Cu2+ doped Fe₃O₄ nanoparticles showed enhanced photocatalytic degradation of MB and EBT dyes, coupled with strong antimicrobial activity due to improved light absorption and charge separation [40]. The ZrO₂/PANI nanocomposite exhibits superior photocatalytic performance for rapid degradation of Carbol Fuchsin dye, showing improved properties over individual components [41]. Similarly, ZnO/CuO nanocomposites efficiently degrade organic dyes due to enhanced charge separation and visible light absorption, while also serving as sensitive NO₂ gas sensors [42]. The TiO₂-ZrO₂-PANI nanocomposite further enhances water purification by combining high photocatalytic activity, large surface area, and effective charge transfer, offering a durable and sustainable material for dye removal under visible light [43]. Ternary metal oxide (TMO) nanocomposites exhibit unique physicochemical properties due to the synergistic interaction of three metal oxides. Systems like CuO/ZrO2/Al2O3 offer high surface area, tunable band gap, and efficient charge separation through heterojunction formation, which suppresses electron-hole recombination and enhances photocatalytic performance.

In this study, we conducted an electrochemical method for the synthesis of $\text{CuO/ZrO}_2/\text{Al}_2\text{O}_3$ nanocomposite and characterized the obtained material with various analytical techniques. In this context, the $\text{CuO/ZrO}_2/\text{Al}_2\text{O}_3$ nanocomposite offers several advantages. CuO, with its narrow band gap, enhances visible light absorption and promotes electron transfer. ZrO_2 contributes excellent thermal and chemical stability, while Al_2O_3 provides a high surface area and serves as a stable support for uniform dispersion of active sites. The synergistic combination of these oxides not only suppresses charge recombination but also improves the adsorption of dye molecules

and enhances reactive oxygen species (ROS) generation. The novelty of this work lies in the green electrochemical synthesis of a $\rm CuO/ZrO_2/Al_2O_3$ ternary heterojunction photocatalyst that uniquely combines high surface area, efficient charge separation, and visible-light activity, enabling dual photocatalytic and antimicrobial functionality.

2. Materials and methodology

2.1. Materials and characterization

Elico Pvt Ltd. supplied the platinum electrode, Alfa Asear gave the sodium bicarbonate, and Alfa Asear furnished the Zirconium, copper and aluminum metal wires. Every experiment used deionized water from the PURELAB extreme water purification system. No additional purification occurred and all chemicals were used exactly as supplied.

SEM analysis was carried out on a ZEISS SEM microscope, modelevo/IS 15, Tokyo, Japan. Micrographs were taken at 5 kV and composites were coated with graphite before analysis. An UV-Vis Shimadzu UV-1800 instrument, with optical cell length 10 mm and cellvolume-3mL,was used for absorbance analysis. Composite XRD analysis was performed on a Rigaku desktop miniplex II X-ray powder diffractometer with Cu K α radiation, (1.5406 Å) as the energy source. An atomic absorption spectroscopy (model number GBC, Avanta version 1.31) analysis was carried out for the quantitation of metals in organic matrices.

2.2. Methodology

2.2.1. Electrochemical synthesis of CuO/ZrO₂/Al₂O₃ nanocomposite

CuO/ZrO₂/Al₂O₃ nanocomposites were synthesized electrochemically in a two-electrode setup using platinum foil (cathode, 99.9 % purity) and aluminum, copper, and zirconium wires (≥99 % purity, anodes). The electrodes (≈3 cm² area, 3 cm apart) were immersed in 30 mL of 0.5 % NaHCO₃ solution (pH ≈ 8.3) and electrolyzed at room temperature for 6 h under constant stirring, with the current maintained at 20 mA (≈6.7 mA cm²). During electrolysis, Al³ , Zr⁴ , and Cu² ions were released from the anodes and oxidized to form their respective oxides, with deposition rates influenced by their reduction potentials (Al: −1.66 V, Zr: −1.53 V, Cu: +0.34 V). Because of its more negative potential, Al³ ioxidized more readily than Zr⁴ and Cu² favoring the initial formation of Al₂O₃ followed by ZrO₂ and CuO. The bicarbonate medium acted as a mild buffer, stabilizing pH during electrolysis and preventing uncontrolled precipitation.

After synthesis, the product was repeatedly washed with distilled water to remove excess electrolytes and centrifuged to collect the precipitate. The dried material was then calcined at 700 °C for 2 h at a heating rate of 10 °C/min, which improved crystallinity and removed residual sodium and hydroxide impurities. Minor trace metal impurities present in the starting wires were negligible, as confirmed by the absence of extraneous peaks in XRD and EDX analysis. The combination of oxides in a single composite structure arises from the simultaneous oxidation of the three anode metals under the applied current. This electrochemical approach provides a simple, reproducible, and environmentally friendly method for preparing ternary metal oxide nanocomposites.

$$2NaHCO_3 + 2e^- \rightleftharpoons 2Na + 2CO_2 + 2OH^-$$

$$Zr \rightleftharpoons Zr^{4+} + 4e^- Cu \rightleftharpoons Cu^{2+} + 2e^- Al \rightleftharpoons Al^{3+} + 3e^-$$

$$Zr^{4+} + 4(OH)^- \rightleftharpoons Zr(OH)_4 Cu^{2+} + 2(OH)^- \rightleftharpoons Cu(OH)_2 Al^{3+} + 3(OH)^- \rightleftharpoons Al(OH)_3$$

$$Cu(OH)_2 + Zr(OH)_4 + 2Al(OH)_3 \rightleftharpoons CuO/ZrO_2/Al_2O_3 + 6H_2O$$

2.2.2. Photodegradation of Indigo Carmine dye using $\text{CuO/ZrO}_2/\text{Al}_2\text{O}_3$ under sunlight

The photodegradation of Indigo Carmine (IC) dye using CuO/ZrO₂/ Al₂O₃ under sunlight was investigated by preparing a solution of IC dye with a defined concentration (0.0-50 ppm) in de-ionized water. Adsorption-desorption equilibrium was established by dispersing a specified quantity of CuO/ZrO₂/Al₂O₃ nanocomposite catalyst in the dye solution and stirring it in the dark for 15-30 min. In a photocatalytic reactor, the solution is then continuously stirred while exposed to sunlight. To monitor dye degradation, aliquots of the solution are taken out at regular intervals, centrifuged to remove the catalyst and then evaluated with a UV-Visible spectrophotometer at wavelength 610 nm. By altering the catalyst dosage, pH, starting dye concentration, and irradiation duration, optimization experiments can be carried out. Additionally, recovering, cleaning and reusing the catalyst in subsequent degradation cycles can be used to verify its reusability. The photocatalytic degradation experiments were conducted in triplicate under identical conditions to ensure reproducibility. The results showed consistent degradation efficiencies with only minor variations ($\pm 3\%$), confirming the repeatability of the process.

2.2.3. Biological activity

2.2.3.1. Anti-bacterial activity. To assess their antibacterial effectiveness, on the produced CuO/ZrO2/Al2O3 was tested against a few Gram-positive and Gram-negative pathogens. This study included Gram-positive bacterial strains, such as Listeria monocytogenes (ATCC 13593), Staphylococcus aureus (ATCC 700699) and Bacillus subtilis (ATCC 21332) as well as Gram-negative strains, such as Pseudomonas aeruginosa (ATCC10145). The inoculum suspension was standardized to include 106 bacterial colonyforming units. Separate stock solutions of each synthesized CuO/ZrO₂/ Al₂O₃ (1 mg/mL) were made in dimethylsulfoxide (DMSO, v/v). The bacterial activity was investigated using the well diffusion method [44]. Using a sterile L-shaped glass rod, the produced bacterial inoculums were equally distributed over a Muller-Hinton agar plate.100 µL of the test composite was added to each well after the wells (9 mm in diameter) were prepared using a sterile cork borer. Each plate was then incubated for one day at 37 °C. Following incubation, the zone of inhibition (in millimeters) was measured on each well.

2.2.3.2. Antifungal activity. The synthesized CuO/ZrO $_2$ /Al $_2$ O $_3$ was tested for its invitro antifungal activity using the disc diffusion method. Aspergillusflavus and Aspergillusniger were used in this investigation and were cultivated on potato dextrose agar (PDA). The standard process involved creating a well in the middle of the agar medium, which had already been inoculated with fungi and it had a diameter of around 9 mm. Using a micro pipette, the tested solutions (100 μ L) were carefully added to the plate, which was then incubated for three days at 37 °C. Diffusion of the test solution and the growth of the infected fungi occurred in the interim. On the plate, track the inhibitory zone's growth. For the investigation, fluconazole served as a reference chemical.

2.2.3.3. Minimum inhibitory concentration. The resultant CuO/ZrO₂/Al₂O₃ screen is used for the serial plate dilution method's MIC test in DMSO. In the nutrient broth, which includes logarithmic serially diluted magnitudes of the test nanocomposite and controls, 10^4 c.f.u mL $^{-1}$ (colony composing unit) of actively proliferating bacterial cells were injected. Microbial cultures were incubated at 37° C for 24 h and their optical density (OD) was measured at 600 nm using spectrophotometry and ocular inspection. The term minimum inhibitory concentration (MIC) refers to the lowest concentration (highest dilution) needed to observe the bacterial magnification.

2.2.3.4. Antioxidant activity. The absorption peak of DPPH, which has an odd electron, is located at 517 nm. The DPPH moiety unpaired electron pairs off, causing a stoichiometric drop in absorbance in relation to the quantity of electrons used. This change in absorbance from the resulting

reaction has been very helpful in determining how well a number of compounds can scavenge free radicals. DPPH was utilized to test the compounds' free radical-scavenging activity in the hydrogen-donating or radical-scavenging ability by giving the stable radical [45]. To create the sample stock solutions (1 mg/mL), an appropriate amount of DPPH was dissolved in DMSO. Stock solutions were subjected to concentration changes (0.2–1.0 $\times 10^{-2}~\mu L$) up to 3 mL with methanol. For the above-tested solution, DPPH solution was used. After giving the resultant combination a good shake and letting it sit for half an hour, the absorbance at 517 nm was measured. Every estimate was performed three times and the findings were expressed as mean \pm standard deviation (S.D.). The experiment's standard or positive was ascorbic acid, which was utilized as the negative control in parallel with the test compound and without the test compound or standard. The ability to scavenge the DPPH radical was determined using the following formula:

 $I (\%) = (A_{blank} - A_{sample} / A_{blank}) \times 100,$

Where A_{sample} is the absorbance of the test compounds and A_{blank} is the absorbance of the control reaction mixture including the test compounds.

3. Results and discussion

3.1. X-ray diffraction (XRD)

Fig. 1a displays the XRD pattern of the synthesized CuO/ZrO $_2$ /Al $_2$ O $_3$ nanocomposite, which exhibits unique diffraction peaks. The 20 values of the peaks 30.2° and 34.8°, which correlate to crystal planes of the (hkl) values (101) and (110) respectively, verify the presence of ZrO $_2$ [JCPDS No. 17–0923] [46]. The 20 values of 35.5°, 38.7°, 58.3°, 61.5° and 68.1°, which correlate to the crystal planes of the (hkl) values (-111), (111), (202), (-113) and (220) respectively, verify the presence of CuO [JCPDF No. 48–1548] [47]. The 20 values 32.6°, 37.2°, and 54.2°, which correlate to the crystal planes of the (hkl) values (220), (222) and (422), respectively, show the presence of Al $_2$ O $_3$ [JCPDF No. 10–0173] [48]. By the Scherrer equation the average crystallite sizes of CuO/ZrO $_2$ /Al $_2$ O $_3$ nanocomposite was found to be 51.5 \pm 0.7 nm.

3.2. The energy dispersive X-ray spectroscopy (EDX)

The exhibited Energy Dispersive X-ray Spectroscopy (EDX) spectrum is used to qualitatively and quantitatively examine the sample elemental composition. The EDX spectrum in Fig. 1b confirms the presence of O, Al, Zr, and Cu. The most abundant element, oxygen, is 49.5 wt percent and exhibits substantial oxidation. In the inset of Fig. 1b, the atomic mass percentages of Al (17.3 %), Zr (15.5 %), and Cu (17.7 %) suggest that a metal oxide CuO/ZrO₂/Al₂O₃ nanocomposite may be formed. The peaks at 0.52 keV (O), 1.5 keV (Al), 15.8 keV (K shell of Zr), 2.0 keV (L shell of Zr) and 8 keV (Cu) verify their presence. CuO, Al₂O₃ and ZrO₂ are among the oxides that could be produced due to the high oxygen level. The inset in Fig. 1b shows the percentage of atoms and weights.

3.3. Scanning electron microscope images (SEM)

A heterogeneous and agglomerated surface morphology, characteristic of multi-phase nanomaterials is revealed by the SEM images Fig. 1c and Fig. 1d of the $\text{CuO/ZrO}_2/\text{Al}_2\text{O}_3$ nanocomposite. The electrochemical approach was used to carry out the synthesis, which allowed CuO and ZrO_2 to be uniformly deposited onto the Al_2O_3 surface. Strong interparticle interactions are shown by the irregularly shaped and closely packed particles. On the Al_2O_3 matrix, CuO and ZrO_2 are heterogeneously joined to form a stable composite structure. Because of the high surface energy and insufficient dispersion during synthesis, agglomeration is clearly visible. The surface area and catalytic potential of the composite are increased by its rough and porous appearance.

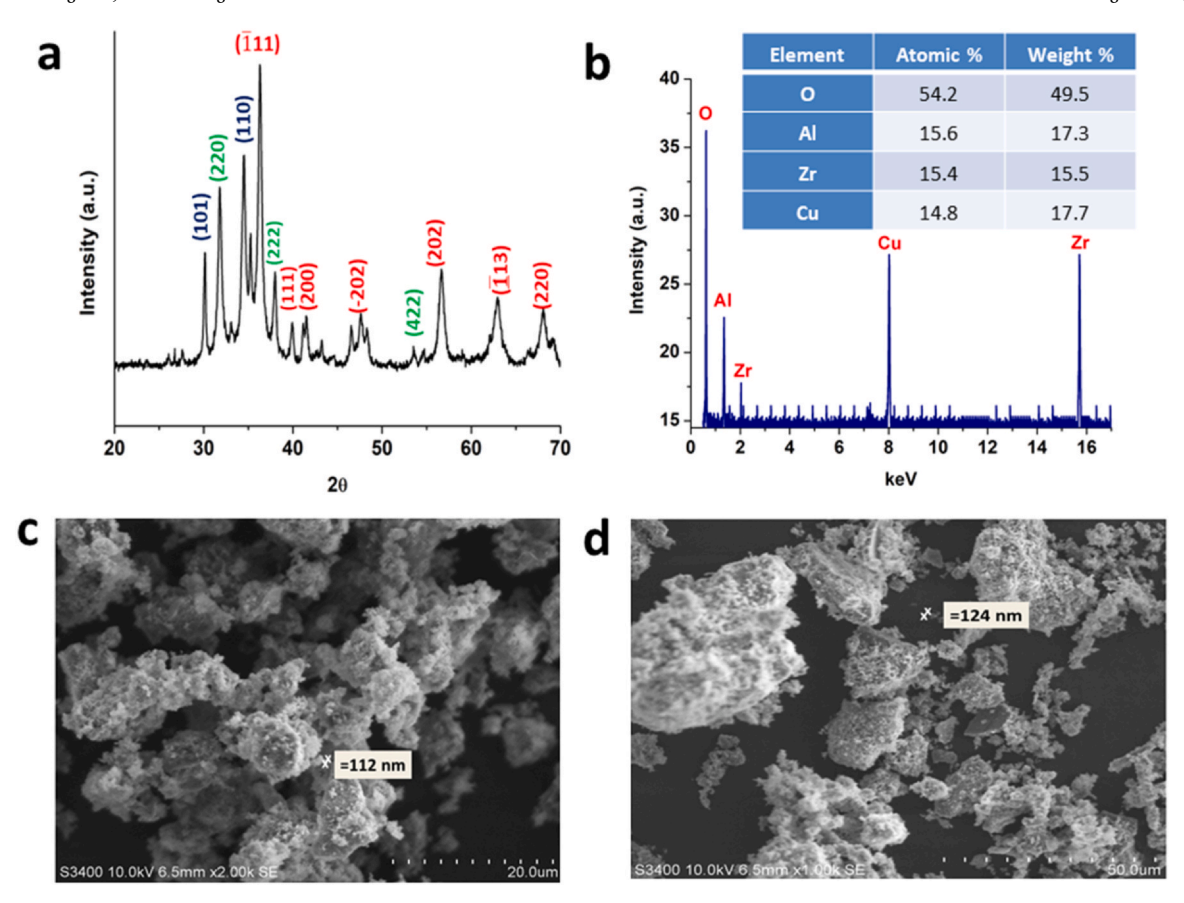


Fig. 1. a) X-ray diffraction pattern b) Energy Dispersive X-ray Spectroscopy (EDX) c) and d) Scanning Electron microscope images of $CuO/ZrO_2/Al_2O_3$ nanocomposite.

Different phases are suggested by bright and dark contrasts with $\rm ZrO_2$ and $\rm CuO$ seeming brighter and $\rm Al_2O_3$ appearing darker. The successful integration of all three oxides is confirmed by nanoscale characteristics. Grain boundaries and porous areas suggest strong potential for adsorption or photocatalysis. All things considered, the SEM validates the creation of a functionally organized and well-blended nanocomposite.

3.4. Transmission electron microscopy analysis

The TEM micrographs (Fig. 2a and b) of the CuO/ZrO₂/Al₂O₃ nanocomposite reveal well-defined, nearly spherical nanoparticles with a uniform size distribution in the range of 50-100 nm. The particles display a distinct core-shell-like contrast, suggesting a hybrid interfacial structure where CuO and ZrO2 nanoparticles are effectively anchored on the Al2O3 matrix. The darker regions correspond to the CuO and ZrO2 phases, while the lighter areas indicate the Al₂O₃ support, confirming the successful formation of a ternary nanocomposite. The close contact between the constituent oxides implies the creation of heterojunction interfaces, which facilitate charge separation and efficient electron transfer during photocatalysis. The uniform morphology and interconnected network structure contribute to the high surface area and porosity, as supported by BET analysis. Such a nanostructured arrangement provides abundant active sites for adsorption and reaction, enabling enhanced photocatalytic degradation of Indigo Carmine dye. The TEM results therefore demonstrate that the CuO/ZrO2/Al2O3 composite possesses a well-integrated hybrid structure suitable for efficient visible-light-driven photocatalysis.

3.5. BET surface area analysis

The specific surface areas (SBET) of pure Al_2O_3 and the synthesized catalysts (CuO/ZrO $_2$ /Al $_2O_3$) were determined from nitrogen

adsorption-desorption isotherms (type IV) measured at 77 K using a NOVA 3200 BET surface area analyzer (Quantachrome Corporation, USA). Prior to the measurements, all samples were degassed under vacuum at 300 °C for 3.0 h to remove adsorbed species. The surface area was calculated using the Brunauer-Emmett-Teller (BET) method, and no BJH or other pore size distribution analyses were employed in this study. The nitrogen adsorption-desorption isotherms of Al₂O₃ and CuO/ZrO₂/ Al₂O₃ nanocomposite are shown in Fig. 2.c). Both samples exhibit a type IV isotherm with an H3-type hysteresis loop, characteristic of mesoporous materials. The pure Al₂O₃ shows a higher BET surface area of 195 m²/g, while the CuO/ZrO₂/Al₂O₃ nanocomposite displays a slightly reduced surface area of 150 m²/g, attributed to the partial filling of Al₂O₃ pores by CuO and ZrO2 nanoparticles. Despite the decrease, the composite retains a high specific surface area and well-developed porous network, which are beneficial for catalytic reactions. The incorporation of CuO and ZrO2 forms a hybrid structure with intimate interfacial contact, promoting efficient charge separation and enhanced light absorption. These interfacial heterojunctions enable better accessibility of active sites and facilitate the adsorption of dye molecules. Consequently, the high surface area and mesoporous texture of the CuO/ZrO₂/Al₂O₃ nanocomposite play a crucial role in improving photocatalytic degradation efficiency of Indigo Carmine dye, by providing a large reaction interface and accelerating redox processes under light irradiation.

3.6. Rate constant and order of photodegradation reaction

The kinetic of photocatalytic decolorization for most organic compounds is described by the pseudo-first-order kinetic model [49] in (Eq. 1). The blank experiment (control) performed in the absence of the photocatalyst showed no IC dye degradation (data not shown) even after 2 h of irradiation exposure.

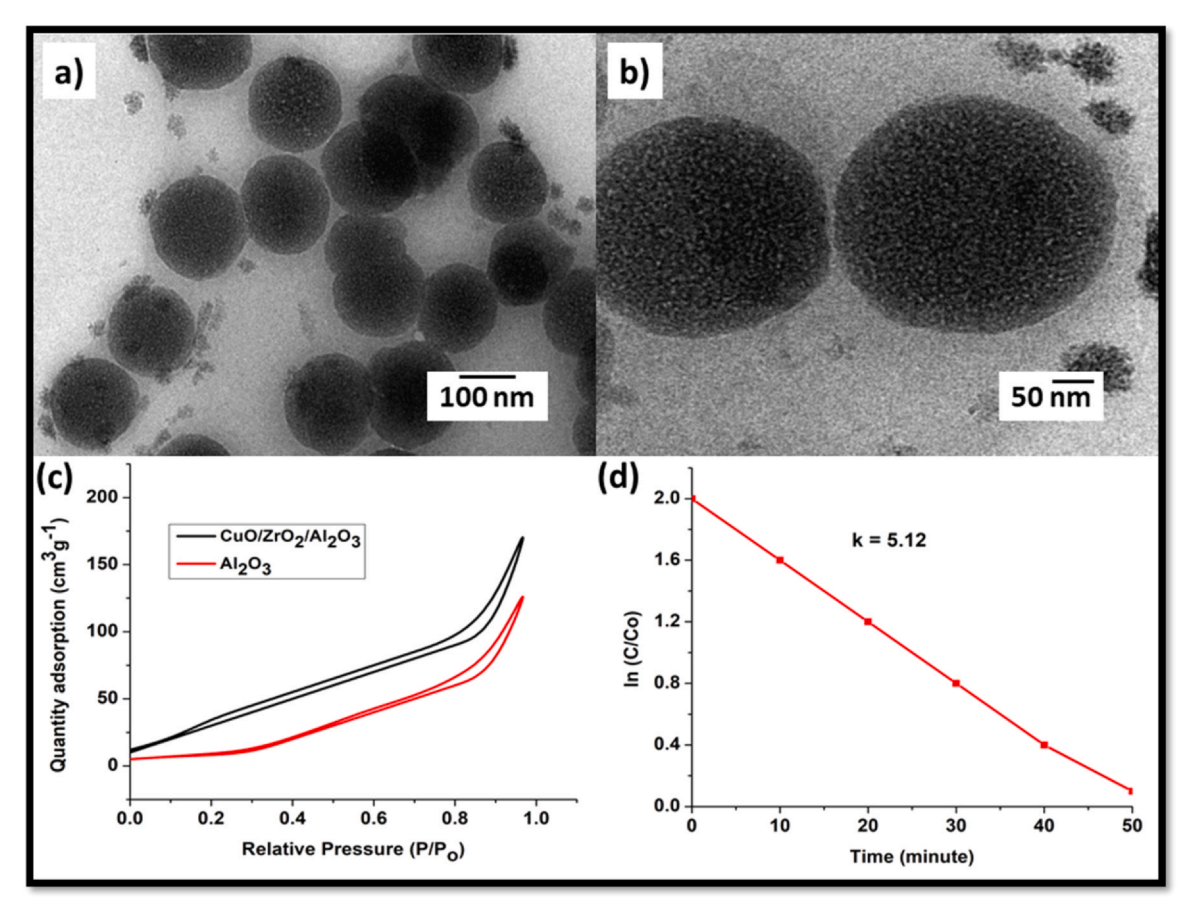


Fig. 2. a) and b) TEM images of $CuO/ZrO_2/Al_2O_3$ nanocomposite c) BET surface area of $CuO/ZrO_2/Al_2O_3$ nanocomposite d) rate constant for the degradation of indigo carmine dye using $CuO/ZrO_2/Al_2O_3$ nanocomposite.

$$\frac{-dc}{dt} = k_{app}C.....$$
 (1)

where $k_{\rm app}~({\rm min}^{-1})$ is the apparent rate constant. In this case, the relation between concentration found at time t (C_t) and the initial concentration (C_0) can be calculated by integrating Eq. (1), considering the limit condition $C_t = C_0$ at t = 0 (Eq. 2).

$$\ln\left(\frac{Co}{Ct}\right) = k_{app}t...$$
(2)

The k_{app} of each experiment was then estimated by plotting ln(Co/Ct) versus reaction time t. At extreme tested pH conditions, pH = 6.5, the kinetic data fit the pseudo-first order. Finally, at pH = 6.5 was the instance with the higher kinetic constant rate (5.12 \times 10⁻² min⁻¹).

3.7. UV-visible spectroscopy

Fig. 3a shows the absorption peak at 525 nm in the CuO/ZrO $_2$ /Al $_2$ O $_3$ nanocomposite UV-Vis absorption spectra indicates effective visible light absorption. The CuO component is mainly responsible for this peak since it displays distinctive d–d transitions of Cu 2 + ions. Good integration of the three oxides and potential synergistic interactions are suggested by the broad absorption band. While Al $_2$ O $_3$ serves as a steady support, ZrO $_2$, with its large band gap, contributes mostly in the UV region. The composite photoactive nature is confirmed by the peak's appearance in the visible spectrum. It is possible that the electrochemical synthesis improved electrical interactions and allowed for uniform mixing. Because of its reactivity to visible light, the composite can be used in photocatalytic processes. All things considered, the spectrum attests to the nanocomposite effective production and useful qualities.

3.8. Band gap energy

The optical band gap energy of the CuO/ZrO $_2$ /Al $_2$ O $_3$ nanocomposite is estimated via the Tauc plot. A direct permitted transition is indicated by the horizontal axis being photon energy (h ν , in eV) and the vertical axis being (α hv) 2 . Band gap energy of 2.5 eV is obtained by extrapolating the linear part of the curve in Fig. 3b. This result indicates effective visible light absorption because it is within the visible light range. CuO inclusion lowers the band gap, as seen by the smaller band gap when compared to pure ZrO $_2$ or Al $_2$ O $_3$. The composite photocatalytic activity under visible light is improved by this improvement. The outcome shows that the metal oxides formed a successful nanocomposite with robust electronic interactions.

3.9. Photocatalytic Indigo Carmine Dye (IC) degradation

The percentage degradation of a contaminant over time for CuO/ZrO₂/Al₂O₃ nanocomposite, CuO, ZrO₂ and Al₂O₃ is depicted in the Fig. 3c. About 95 % degradation is reached by the CuO/ZrO₂/Al₂O₃ nanocomposite (black squares) after 25 min, after which it plateaus. Similar degradation is reached by CuO (red circles), albeit a little later than by the nanocomposite. Degradation is slower for ZrO₂ (blue triangles) and Al₂O₃ (magenta triangles). All materials degrade quickly at first, then gradually toward their ultimate deterioration. The nanocomposite increased activity indicates that its constituent parts work in concert. This demonstrates CuO/ZrO₂/Al₂O₃ capacity for effective photocatalysis.

A contaminant photocatalytic degradation over time for CuO, ZrO_2 , Al_2O_3 and a $CuO/ZrO_2/Al_2O_3$ nanocomposite is depicted in the Fig. 3d. The ratio of the contaminant concentration with time to the initial concentration (C_1/C_0) on the y-axis represents degradation efficiency.

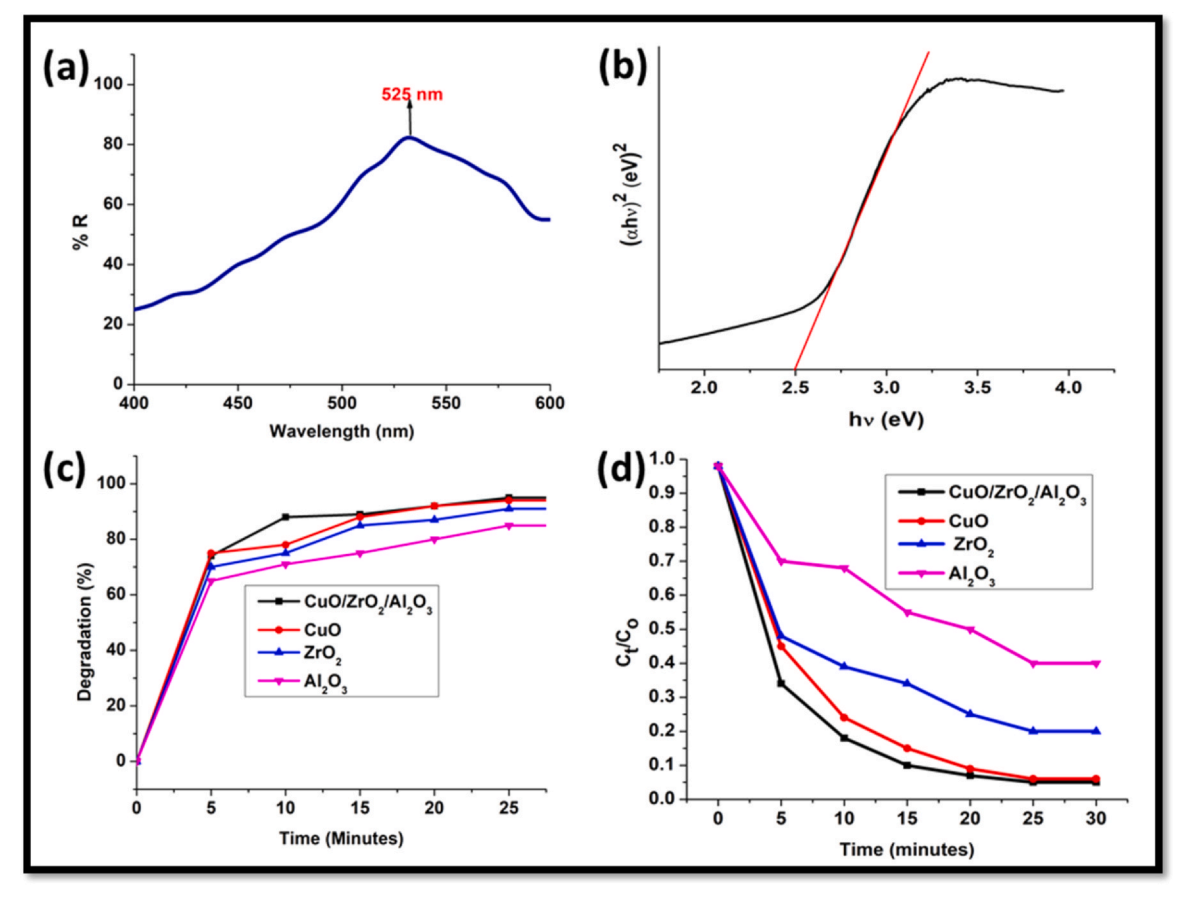


Fig. 3. a) UV-Visible Spectroscopy, b) Band Gap Energy, c) Photocatalytic properties, d) Percentage degradation of IC Dye using CuO/ZrO₂/Al₂O₃ nanocomposite.

The $\text{CuO/ZrO}_2/\text{Al}_2\text{O}_3$ nanocomposite (black squares) degrades at the fastest rate, being nearly completely degraded within about half an hour. In contrast to the nanocomposite, CuO (red circles) exhibits noticeable deterioration, albeit more slowly. The degradation efficiencies of ZrO_2 (blue triangles) and Al_2O_3 (magenta triangles) are lower, with Al_2O_3 being the least. This suggests that the components synergistic interactions improve photocatalytic performance in the nanocomposite. The findings imply that the photocatalytic degradation efficiency is enhanced by the combination of CuO, ZrO_2 and Al_2O_3 .

3.10. Effect of catalytic concentration

The smallest quantity of catalyst required for efficient dye degradation is known as the catalytic minimum concentration. In this investigation, indigo carmine dye was effectively broken down by 0.7 g of the $\text{CuO/ZrO}_2/\text{Al}_2\text{O}_3$ nanocomposite in 25–30 min when exposed to sunshine display in Fig. 4a. The composite absorb great light and reactive species formation provides this high efficiency at a low dosage, which makes it affordable and appropriate for environmental applications.

3.11. Effect of dye concentration

In Fig. 4b shows high catalytic efficiency is demonstrated by the $\text{CuO/ZrO}_2/\text{Al}_2\text{O}_3$ nanocomposite ability to degrade dye up to 95 % at a concentration of 25 ppm. The nanocomposite has enough active surface area to interact with dye molecules at this concentration. Because it breaks down the dye structure by producing reactive oxygen species like hydroxyl and superoxide radicals, the CuO component is essential for catalytic or photocatalytic reactions. Concurrently, ZrO_2 and Al_2O_3 improve the composite's thermal and structural stability and aid in

better dispersion of CuO, which raises the element's availability for catalytic process. These metal oxides work together to effectively degrade dyes, which makes the nanocomposite a viable material for waste water treatment and environmental cleanup applications.

3.12. Effect of pH on Indigo Carmine (IC) dye degradation

The CuO/ZrO $_2$ /Al $_2$ O $_3$ nanocomposite dye degradation is often effective at pH 6.5 because the slightly acidic to neutral pH promotes the generation of reactive oxygen species, especially hydroxyl radicals, without significantly deactivating the catalyst shows in Fig. 4c. Adsorption and subsequent photocatalytic breakdown are facilitated by the nanocomposite's surface maintaining a balanced charge at this pH, which permits good interaction with the majority of dye molecules. Moreover, pH 6.5 is a good pH for stable and effective dye degradation because it avoids the severe circumstances that could otherwise prevent radical generation or lead to dye molecules aggregating.

3.13. Effect of temperature on indigo carmine (IC) dye degradation

The CuO/ZrO $_2$ /Al $_2$ O $_3$ nanocomposite does not significantly degrade or undergo phase shifts at 35 °C in Fig. 4d. CuO remains in its oxidized state, whereas zirconia and alumina maintain their structural integrity. Catalytic activity might go up a little, but there are no significant impacts like sintering or reduction. While dye degradation is conceivable, it happens more slowly than at higher temperatures. All things considered, 35 °C is a reasonable temperature at which the nanocomposite should remain stable and experience no deterioration or change in performance.

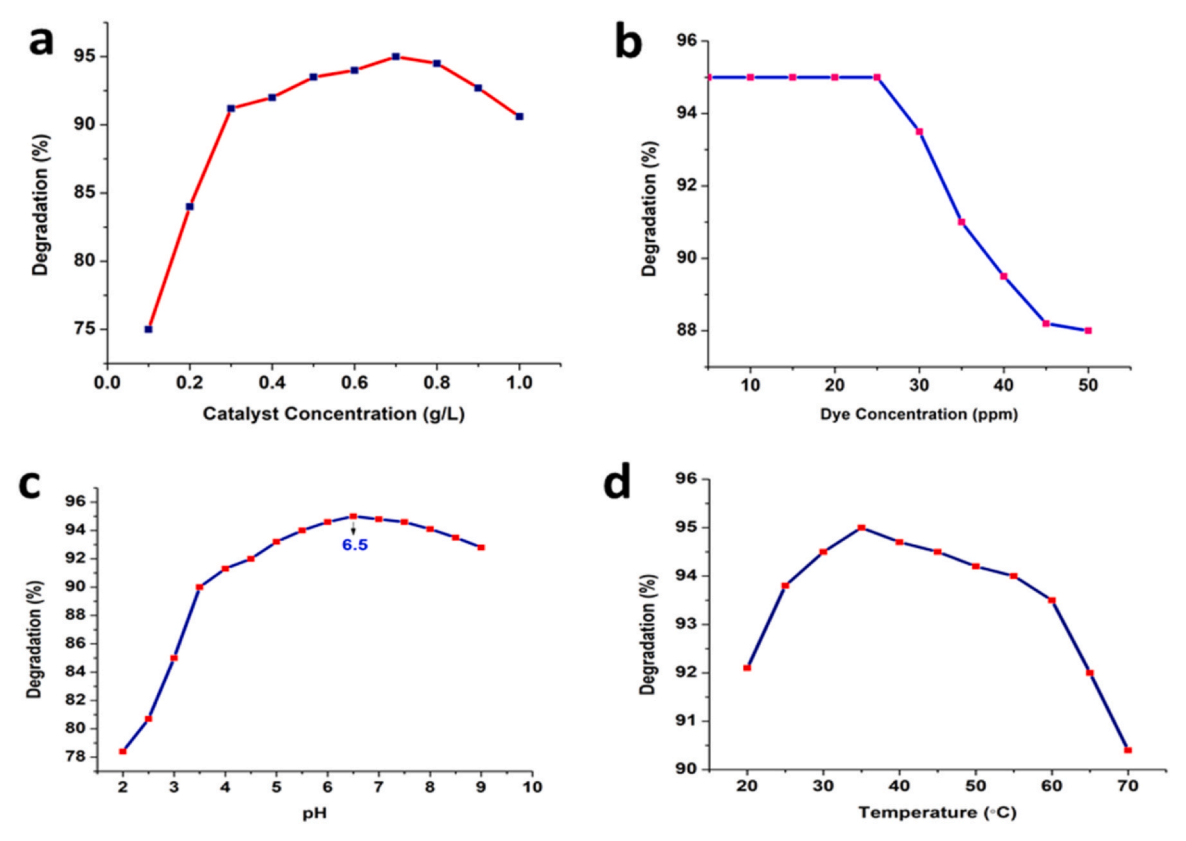


Fig. 4. a) Effect of Catalytic concentration, b) Effect of Dye concentration, c) Effect of pH, d) Effect of Temperature on IC dye degradation.

3.14. Radical-scavenging analysis

To confirm the role of various reactive oxygen species (ROS) in the degradation of Indigo Carmine, radical-scavenging tests were performed using different scavengers. IPA (1 mM), BQ (1 mM), and AO (1 mM) were used as scavengers for 'OH, O_2 ', and h', respectively. As shown in Fig. 5a, the degradation efficiency of IC was 95 % (without scavenger), 73 % (with IPA), 52 % (with BQ), and 68 % (with AO). The significant suppression of degradation in the presence of BQ confirms that O_2 — radicals are the primary reactive species, while 'OH and h' play secondary roles in the photocatalytic mechanism of CuO/ZrO $_2$ / Al $_2$ O $_3$. The results suggest that photogenerated electrons in the conduction band react with adsorbed O $_2$ to form O $_2$ —, which predominantly oxidizes the dye molecules, leading to their degradation.

3.15. Catalyst reusability/cycle performance

The $\text{CuO/ZrO}_2/\text{Al}_2\text{O}_3$ nanocomposite exhibits outstanding reusability, retaining over 95% degradation efficiency after 10 cycles (Fig. 5b). This

confirms its stability and potential for repeated use in photocatalytic applications, making it a cost-effective and durable catalyst for environmental remediation. This has now been clarified in the revised manuscript.

3.16. Mechanism of $CuO/ZrO_2/Al_2O_3$ composite in photocatalytic degradation

The CuO/ZrO₂/Al₂O₃ composite exhibits significant potential for visible light driven photocatalysis, particularly in the region of the solar spectrum ranging from approximately 400–800 nm. This is primarily attributed to the narrow band gap of CuO ($\sim\!1.5$ eV), which allows it to absorb photons in the visible region effectively, while the presence of ZrO₂ aids in charge separation and Al₂O₃ contributes to structural stability and dispersion of active sites. Indigo Carmine (organic pollutant) is used to assess the photocatalytic activity of synthesized specimens upon exposure to visible light. For comparison, the photo catalytic activity of the pure CuO, ZrO₂ and Al₂O₃ were also measured. Al₂O₃ alone show a very low photocatalytic activity 78 %. This low

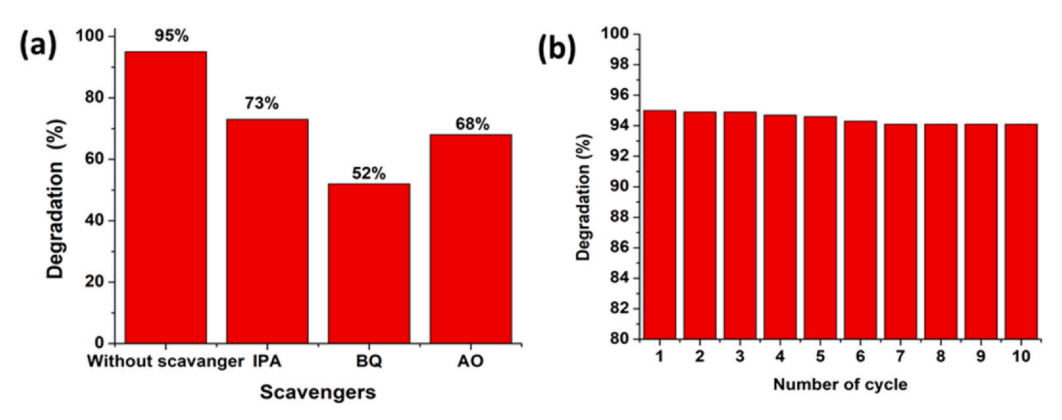


Fig. 5. a) Radical Scavenger test of CuO/ZrO₂/Al₂O₃, b) CuO/ZrO₂/Al₂O₃ Catalyst reusability on IC dye degradation.

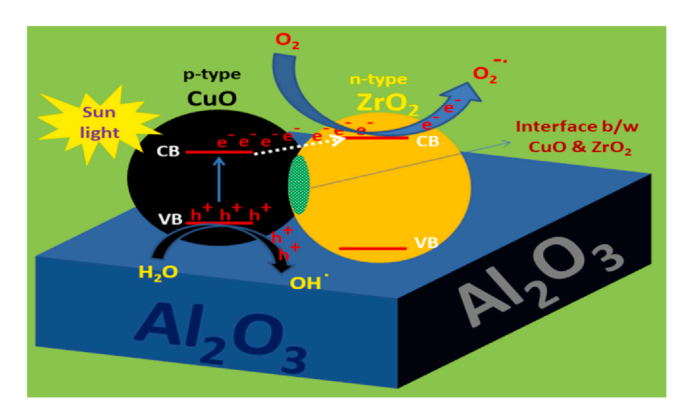


Fig. 6. Schematic mechanisms of IC dye degradation under sunlight using ${\rm CuO/ZrO_2/Al_2O_3}$ nanocomposite.

photocatalytic activity is due to large band gap which makes it less effective harvester of solar light and that is the drawback of ${\rm Al}_2{\rm O}_3$ for the use of sunlight.

During the experiment the sunlight energy was absorbed by the CuO nanoparticle, the energy able to excite electron from valence band of CuO to conduction band of CuO. Therefore electron (e) moved to conduction band and hole (h') present in valence band. Sometimes the formed hole (h') and electron (e) recombined, the degradation efficiency will be decreased due to unavailability of hole (h') and electron (e) for the photocatalysis. Therefore the presence of ZrO₂ helps to separate the hole and electron by interfacial charge separation via p–n heterojunction with CuO and ZrO₂. When the hole (h') and electron (e) get separated by ZrO₂ (n-type Semiconductor) the photodegradation efficiency of the CuO/ZrO₂/Al₂O₃ composite increase to 95 %. The Al₂O₃ nanoparticle with large surface area was helpful for the better dispersion of CuO and ZrO₂ nanoparticle, reduced agglomeration and acts as physical barrier by minimizing recombination effect.

The photogenerated (Excited) electrons from ZrO₂ react with dissolved oxygen to form superoxide radicals. Meanwhile, photogenerated holes (now in CuO) can oxidize water or hydroxide ions to form hydroxyl radicals. These radicals are highly reactive and non-selectively degrade organic IC dyes. The generated radicals attack the Indigo Carmine dye molecules, breaking down their chromophoric structures finally to form H₂O and CO₂. An illustration of p-n heterojunction between CuO and ZrO₂ behavior is proposed as shown in Fig. 6.

When the CuO/ZrO₂/Al₂O₃ system is irradiated under sunlight ($\lambda > 400$ nm), CuO can be activated since the band gap energies of ZrO₂, CuO and Al₂O₃ observed in this study were 5.3, 2.1 and 5.6 eV respectively. The electrons will then react with oxygen molecules to finally form radicals. These radicals will further oxidize the IC molecules that are preferentially adsorbed on the CuO/ZrO₂/Al₂O₃ particles. This is due to the fact that the CuO/ZrO₂/Al₂O₃ particles possess a slightly positive surface charge (at pH 6.5), which would preferably adsorb an ionic dye molecules, rather than cationic dye. As a result, more efficient charge-carrier separation and thus improved photocatalytic activity could be achieved.

Cumulative mechanism:

To highlight the efficiency of the synthesized CuO/ZrO $_2$ /Al $_2$ O $_3$ composite, its photocatalytic degradation performance toward Indigo Carmine (IC) dye was compared with various reported catalysts (Table 1). It can be observed that catalysts such as Bi $_2$ MoO $_6$, Sm 3 -doped ZnS, ZnO-Cu $_2$ O/GO, ZnO nanoparticles, CaZrO $_3$, and ZnBi $_2$ O $_4$ /rGO hybrids exhibit degradation efficiencies ranging from \sim 88% to \sim 96% under UV, visible, or solar irradiation. The present CuO/ZrO $_2$ /Al $_2$ O $_3$ composite demonstrated 95% degradation in 25 min under Sun light, which is comparable or superior to many reported systems. The enhanced activity can be attributed to the synergistic interaction between CuO, ZrO $_2$, and Al $_2$ O $_3$ phases that promotes efficient charge separation and visible-light absorption, reducing electron–hole recombination and improving photocatalytic efficiency.

3.17. Biological activity

3.17.1. Antimicrobial activity

The newly synthesized composite was tested in an *in vitro* antibacterial assay against *B. subtilis, L. monocytogenes, S. aureus and P. aeruginosa*. Additionally, invitro antifungal activity was assessed by assessing two fungi, *A. flavus*and *A. niger*. The area surrounding each well was visually inspected (Fig. 7) to determine the prime range of the zone of inhibition. The zone size in millimeters (mm) was used to quantify the zone of inhibition surrounding each well. Inhibitions against Gram-positive and Gram-negative bacteria are quantified and summarized in Table 2.

3.17.2. Minimum inhibitory concentration

The resulting nanocomposite minimum inhibitory concentration (MIC) was calculated by growing the bacterial cultures overnight, adjusting the concentration, and using the McFarland turbidity standard. To determine the MIC of CuO/ZrO₂/Al₂O₃in the microtitre plate assay, the serial dilution method was used. Both Gram positive and Gram negative bacteria are significantly inhibited by the produced nanocomposite MIC range (Table 3). Significant antibacterial activity was demonstrated by the produced CuO/ZrO₂/Al₂O₃nanocomposite. Since the cell is encased in a lipid membrane, only soluble chemicals are permitted to pass through it, as demonstrated by the Overtone concept of cell permeability. The results obtained clearly imply that the synthesized nanocomposite can be applied to the treatment of resistant microorganisms.

3.17.3. Antioxidant activity

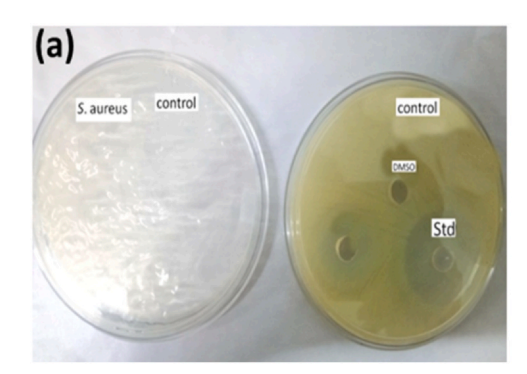
To test the nanocomposite capacity to scavenge free radicals, the DPPH assay was employed. The DPPH assay examined the ability of the resulting nanocomposite to function as an electron transfer in the transformation of the DPPH radical from its radical state to the reduced form, DPPH-H. a 0.1 mM DPPH solution in methanol was prepared as stock, and 1 mL of this solution was mixed with 1 mL of the sample extract at different concentrations. The reaction mixtures were incubated in the dark at room temperature (25 \pm 2 °C) for 30 min to avoid photodegradation. When compared to normal ascorbic acid, the nanocomposite ability to energetically scavenge the DPPH radical was

$$\begin{array}{cccc} CuO + h\gamma & \longrightarrow & e^-_{CB} + h^+_{VB} \\ & e^-_{CB} + O_2 & \longrightarrow & O_2 \\ & & & & \\ h^+_{VB} + H_2O & \longrightarrow & OH + H^+ \\ & O_2 \\ & & & \end{array}$$

$$\begin{array}{c} OH + Indigo \ Carmine & \longrightarrow \ Degraded \ products \ (CO_2, H_2O) \\ & & & \\ \end{array}$$

Table 1
Comparision of Indigo Carmine (IC) dye degradation using various catalysts.

Catalyst	Light source	Time (min)	Degradation (%)	Reference
Bi ₂ MoO ₆	Solar light	120	~94%	[50]
Sm3 * doped ZnS nanoparticles	Visible light (excited at 395 nm)	210	~93 %	[51]
ZnO-Cu ₂ O/Graphene Oxide composite	UV (500 W Hg lamp)	240	96.5 %	[52]
ZnO nanoparticles	UV light	60	~92 %	[53]
CaZrO ₃ -SiO ₂	UV light	90	~96 %	[54]
ZnBi ₂ O ₄ /rGO hybrid	Visible light	75	~91 %	[55]
CuO/ZrO ₂ /Al ₂ O ₃ nanocomposite	Sunlight	25	~95 %	Present work



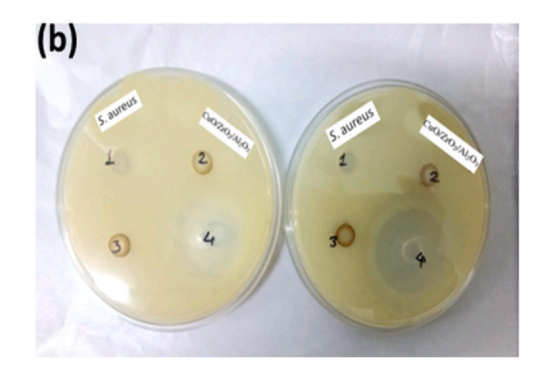


Fig. 7. The bactericidal activity of CuO/ZrO₂/Al₂O₃ nanocomposite and control on S.aureus.

Table 2
Results of antimicrobial activity of as synthesized CuO/ZrO₂/Al₂O₃nanocomposite.

Zone of inhibition (mm) ^a						
Nano composite	Bacteria				Fungi	
	L. Monocytogenes	B. subtilis	S. aureus	E. coli	A. niger	A. flavus
CuO/ZrO ₂ /Al ₂ O ₃	12	7	11	14	14	8
Ampicillin	23	24	25	27	_	_
Fluconazole	-	-	-	-	21	21

The results obtained from the average of three replicates.

Table 3
Minimum inhibitory concentration results.

Nano composite	Bacteria			Fungi		
	L. Monocytogenes	B. subtilis	S. aureus	E. coli	A. niger	A. flavus
CuO/ZrO ₂ /Al ₂ O ₃	93	95	94	97	83	89
Ampicillin	26	26	26	27	-	-
Fluconazole	_	_	_	_	43	43

The results obtained from the average of three replicate analyses

Table 4 Antioxidant ability (IC_{50}) of all the synthesized compounds.

Compounds	$IC_{50} (\mu g/mL) \pm S.D^*$
AA	24 ± 0.55
$CuO/ZrO_2/Al_2O_3$	61 ± 0.29

AA = Ascorbic acid

examined. Its effectiveness was assessed by measuring the absorbance at 517 nm. The reaction mixture color changed from deep purple (DPPH radical) to yellow (DPPH-H), indicating its antioxidant activity. The

decreased absorbance value of the reaction mixture demonstrated the presence of free radical scavenge activity. The $\text{CuO/ZrO}_2/\text{Al}_2\text{O}_3$ nanocomposite IC_{50} value was similar to that of ascorbic acid (Table 4).

4. Summary and conclusion

In this study, a nanoscale $\text{CuO/ZrO}_2/\text{Al}_2\text{O}_3$ ternary nanocomposite was successfully synthesized through a simple, cost-effective, and environmentally benign electrochemical method for dual applications in photocatalysis and bacterial inactivation. The synthesized nanocomposite exhibited outstanding photocatalytic performance toward the degradation of Indigo Carmine dye under natural sunlight

S.D = Standard deviation (average of three replicates)

irradiation. Using only 0.7 g L⁻¹ of the catalyst, a high degradation efficiency of 95 % was achieved under optimized conditions (pH 6.5, 35 °C, 25 ppm dye concentration). The presence of Al₂O₃ provided a stable and porous surface that enhanced dye adsorption, while CuO and ZrO2 formed an efficient heterojunction facilitating effective charge separation. Upon sunlight exposure, photoexcited electrons generated in CuO were transferred to the conduction band of ZrO₂, thereby suppressing electron-hole recombination and enhancing the overall photocatalytic activity. This synergistic interaction among the constituent oxides led to superior adsorption capacity and visible-light responsiveness. In addition to photocatalytic performance, the CuO/ZrO2/Al2O3 nanocomposite displayed remarkable biological activity, including antimicrobial efficacy, minimum inhibitory concentration (MIC), antioxidant potential, and antibacterial properties. Overall, this study demonstrates that the CuO/ZrO₂/Al₂O₃ nanocomposite is a promising multifunctional material for sustainable wastewater treatment and microbial control applications. The novelty of this work lies in the electrochemical synthesis of a ternary CuO/ZrO₂/Al₂O₃ heterostructure that couples high surface area with visible-light activity and biological functionality features rarely achieved together in a single photocatalyst system.

CRediT authorship contribution statement

Jagadish Krishnegowda: Writing – review & editing, Visualization, Conceptualization. Vivekraj Nagaraju: Writing – original draft, Visualization. M N Kumara: Writing – review & editing, Writing – original draft, Visualization, Supervision, Conceptualization. Thriveni Muttegere Karigiregowda: Writing – review & editing, Visualization. Lingegowda Nagarakere Shivalingaiah: Writing – review & editing, Visualization.

Consent to participate

Not applicable

Consent to publish

Not applicable

Ethical approval

This studies has not consent with respect to human and/or animal studies, hence no ethical committee approval has been taken.

Funding

No funding has been granted to this work

Data availability

The article and raw data include the original contributions made in this study. Contacting the corresponding author will provide the data on request.

Declaration of Competing Interest

The authors declare that they have no known competing financial interests or personal relationships that could have appeared to influence the work reported in this paper.

Declaration of generative AI and AI-assisted technologies in the writing process

During the preparation of this work the author(s) used ChatGPT in order to clarification of results. After using this tool/service, the authors reviewed and edited the content as needed and take full responsibility for the content of the publication.

Acknowledgments

The authors are grateful to the University of Mysore and Yuvaraja's College, Mysuru, 570005. Partial analytical support was provided by the Vijnana Bhavana, Mansagangothri, University of Mysore, Mysuru.

References

- M. Nasrollahzadeh, S.M. Sajadi, M. Sajjadi, Z. Issaabadi, An introduction to nanotechnology, Interface Science and Technology 28 Elsevier, 2019 Jan 1, pp. 1–27, https://doi.org/10.1016/B978-0-12-813586-0.00001-8.
- [2] M. Di Ventra, S. Evoy, J.R. HeflinJr (Eds.), Introduction to Nanoscale Science and Technology, Springer US, Boston, MA, 2004 Jun 30, https://doi.org/10.1007/ b119185
- [3] F.C. Adams, C. Barbante, Nanoscience, nanotechnology and spectrometry, Spectrochim. Part B At. Spectrosc. 86 (2013 Aug 1) 3–13, https://doi.org/10.1016/ j.sab.2013.04.004.
- [4] N. Xin, J. Guan, C. Zhou, X. Chen, C. Gu, Y. Li, M.A. Ratner, A. Nitzan, J.F. Stoddart, X. Guo, Concepts in the design and engineering of single-molecule electronic devices, Nat. Rev. Phys. 1 (3) (2019 Mar) 211–230, https://doi.org/10.1038/s42254-019-0022-x.
- [5] I.D. Kuntz, E.C. Meng, B.K. Shoichet, Structure-based molecular design, Acc. Chem. Res. 27 (5) (1994 May 1) 117–123, https://doi.org/10.1021/ar00041a001.
- [6] R. Ballardini, V. Balzani, A. Credi, M.T. Gandolfi, M. Venturi, Artificial molecular-level machines: which energy to make them work? Acc. Chem. Res. 34 (6) (2001 Jun 19) 445–455, https://doi.org/10.1021/ar000170g.
- [7] H. Zhu, W. Luo, P.N. Ciesielski, Z. Fang, J.Y. Zhu, G. Henriksson, M.E. Himmel, L. Hu, Wood-derived materials for green electronics, biological devices, and energy applications, Chem. Rev. 116 (16) (2016 Aug 24) 9305–9374, https://doi.org/10. 1021/acs.chemrev.6b00225.
- [8] E. Oztemel, S. Gursev, Literature review of Industry 4.0 and related technologies, J. Intell. Manuf. 31 (1) (2020 Jan) 127–182, https://doi.org/10.1007/s10845-018-1433-8.
- [9] M.R. Lukatskaya, B. Dunn, Y. Gogotsi, Multidimensional materials and device architectures for future hybrid energy storage, Nat. Commun. 7 (1) (2016 Sep 7) 12647, https://doi.org/10.1038/ncomms12647.
- [10] G. Yu, X. Xie, L. Pan, Z. Bao, Y. Cui, Hybrid nanostructured materials for high-performance electrochemical capacitors, Nano Energy 2 (2) (2013 Mar 1) 213–234, https://doi.org/10.1016/j.nanoen.2012.10.006.
- [11] J. Njuguna, F. Ansari, S. Sachse, V.M. Rodriguez, S. Siqqique, H. Zhu, Nanomaterials, nanofillers, and nanocomposites: types and properties, Health and Environmental Safety of Nanomaterials, Woodhead Publishing, 2021 Jan 1, pp. 3–37, https://doi.org/10.1016/B978-0-12-820505-1.00011-0.
- [12] H.M. Somarathna, S.N. Raman, D. Mohotti, A.A. Mutalib, K.H. Badri, The use of polyurethane for structural and infrastructural engineering applications: a state-ofthe-art review, Constr. Build. Mater. 190 (2018 Nov 30) 995–1014, https://doi.org/ 10.1016/j.conbuildmat.2018.09.166.
- [13] D.B. Dittenber, H.V. GangaRao, Critical review of recent publications on use of natural composites in infrastructure, Composites Part A Applied Science Manufacturing 43 (8) (2012 Aug 1) 1419–1429, https://doi.org/10.1016/j. compositesa.2011.11.019.
- [14] D. Chellaganesh, M.A. Khan, J.W. Jappes, Thermal barrier coatings for high temperature applications—a short review, Mater. Today. Proc. 45 (2021 Jan 1) 1529–1534, https://doi.org/10.1016/j.matpr.2020.08.017.
- [15] T.V. Duncan, Applications of nanotechnology in food packaging and food safety: barrier materials, antimicrobials and sensors, J. Colloid Interface Sci. 363 (1) (2011 Nov 1) 1–24, https://doi.org/10.1016/j.jcis.2011.07.017.
- [16] M.M. Tijani, A. Aqsha, N. Mahinpey, Synthesis and study of metal-based oxygen carriers (Cu, Co, Fe, Ni) and their interaction with supported metal oxides (Al₂O₃, CeO₂, TiO₂, ZrO₂) in a chemical looping combustion system, Energy 138 (2017 Nov 1) 873–882, https://doi.org/10.1016/j.energy.2017.08.099.
- [17] L.E. Briand, A.M. Hirt, I.E. Wachs, Quantitative determination of the number of surface active sites and the turnover frequencies for methanol oxidation over metal oxide catalysts: Application to bulk metal molybdates and pure metal oxide catalysts, J. Catal. 202 (2) (2001 Sep 10) 268–278, https://doi.org/10.1006/jcat.2001.
- [18] R.J. Farrauto, R.M. Heck, Environmental catalysis into the 21st century, Catal. Today 55 (1-2) (2000 Jan 5) 179–187, https://doi.org/10.1016/S0920-5861(99) 00237 0
- [19] J.C. Védrine, The role of redox, acid-base and collective properties and of cristalline state of heterogeneous catalysts in the selective oxidation of hydrocarbons, Top. Catal. 21 (2002 Oct) 97–106, https://doi.org/10.1023/ A:1020560200125.
- [20] F. Seker, K. Meeker, T.F. Kuech, A.B. Ellis, Surface chemistry of prototypical bulk II – VI and III – V semiconductors and implications for chemical sensing, Chem. Rev. 100 (7) (2000 Jul 12) 2505–2536, https://doi.org/10.1021/cr980093r.
- [21] S. Mallakpour, E. Khadem, Carbon nanotube-metal oxide nanocomposites: Fabrication, properties and applications, Chem. Eng. J. 302 (2016 Oct 15) 344–367, https://doi.org/10.1016/j.cej.2016.05.038.
- [22] S. Raza, A. Hayat, T. Bashir, C. Chen, L. Shen, Y. Orooji, H. Lin, Electrochemistry of 2D-materials for the remediation of environmental pollutants and alternative energy storage/conversion materials and devices, a comprehensive review, Sustain. Mater. Technol. (2024 May 8) e00963, https://doi.org/10.1016/j.stmat.2024. 100963.

- [23] H. Wang, X. Yuan, G. Zeng, Y. Wu, Y. Liu, Q. Jiang, S. Gu, Three dimensional graphene based materials: synthesis and applications from energy storage and conversion to electrochemical sensor and environmental remediation, Adv. Colloid Interface Sci. 221 (2015 Jul 1) 41–59, https://doi.org/10.1016/j.cis.2015.04.005.
- [24] M. Nasrollahzadeh, S.M. Sajadi, M. Sajjadi, Z. Issaabadi, An introduction to nanotechnology, Interface Science and Technology 28 Elsevier, 2019 Jan 1, pp. 1–27, https://doi.org/10.1016/B978-0-12-813586-0.00001-8.
- [25] M.C. Roco, M.C. Hersam, C.A. Mirkin, C.A. Mirkin, M. Tuominen, Synthesis, processing, and manufacturing of components, devices, and systems. Nanotechnology Research Directions for Societal Needs in 2020, Retrosp. Outlook (2011) 109–158, https://doi.org/10.1007/s11051-011-0275-5.
- [26] M.H. Saleem, U. Ejaz, M. Vithanage, N. Bolan, K.H. Siddique, Synthesis, characterization, and advanced sustainable applications of copper oxide nanoparticles: a review, Clean. Technol. Environ. Policy (2024 Mar 13) 1–26, https://doi.org/10.10098-024-02774-6.
- [27] J.O. Ighalo, P.A. Sagboye, G. Umenweke, O.J. Ajala, F.O. Omoarukhe, C.A. Adeyanju, S. Ogunniyi, A.G. Adeniyi, CuO nanoparticles (CuO NPs) for water treatment: a review of recent advances, Environ. Nanotechnol. Monit. Manag. 15 (2021 May 1) 100443, https://doi.org/10.2166/wst.2022.153.
- [28] S.S. Chan, S.S. Low, K.W. Chew, T.C. Ling, J. Rinklebe, J.C. Juan, E.P. Ng, P.L. Show, Prospects and environmental sustainability of phyconanotechnology: a review on algae-mediated metal nanoparticles synthesis and mechanism, Environ. Res. 212 (2022 Sep 1) 113140, https://doi.org/10.1016/j.envres.2022.113140.
- [29] H. Bahrulolum, S. Nooraei, N. Javanshir, H. Tarrahimofrad, V.S. Mirbagheri, A.J. Easton, G. Ahmadian, Green synthesis of metal nanoparticles using microorganisms and their application in the agrifood sector, J. Nanobiotechnol. 19 (2021 Dec) 1–26, https://doi.org/10.1186/s11671-021-00552-w.
- [30] C.R. Ferreira, A.A. Santiago, R.C. Vasconcelos, D.F. Paiva, F.Q. Pirih, A.A. Araújo, F.V. Motta, M.R. Bomio, Study of microstructural, mechanical, and biomedical properties of zirconia/hydroxyapatite ceramic composites, Ceram. Int. 48 (9) (2022 May 1) 12376–12386, https://doi.org/10.1016/j.ceramint.2022.01.102.
- [31] F. Ordóñez, F. Chejne, E. Pabón, K. Cacua, Synthesis of ZrO₂ nanoparticles and effect of surfactant on dispersion and stability, Ceram. Int. 46 (8) (2020 Jun 1) 11970–11977, https://doi.org/10.1016/j.ceramint.2020.01.236.
- [32] M. Rahimian, N. Ehsani, N. Parvin, H.R. Baharvandi, The effect of sintering temperature and the amount of reinforcement on the properties of Al–Al₂O₃ composite, Mater. Des. 30 (8) (2009 Sep 1) 3333–3337, https://doi.org/10.1016/j.matdes. 2008.11.027.
- [33] A. Rai, D. Lee, K. Park, M.R. Zachariah, Importance of phase change of aluminum in oxidation of aluminum nanoparticles, J. Phys. Chem. B 108 (39) (2004 Sep 30) 14793–14795, https://doi.org/10.1021/jp0373402.
- [34] P. Khandel, R.K. Yadaw, D.K. Soni, L. Kanwar, S.K. Shahi, Biogenesis of metal nanoparticles and their pharmacological applications: present status and application prospects, J. Nanostructure Chem. 8 (2018 Sep) 217–254, https://doi.org/10.1007/ s40097-018-0267-4
- [35] P. Kuppusamy, M.M. Yusoff, G.P. Maniam, N. Govindan, Biosynthesis of metallic nanoparticles using plant derivatives and their new avenues in pharmacological applications—An updated report, Saudi Pharm. J. 24 (4) (2016 Jul 1) 473–484, https://doi.org/10.1016/j.jsps.2014.11.013.
- [36] M.M. Rahman, M.R. Islam, S. Akash, M. Harun-Or-Rashid, T.K. Ray, M.S. Rahaman, M. Islam, F. Anika, M.K. Hosain, F.I. Aovi, H.A. Hemeg, Recent advancements of nanoparticles application in cancer and neurodegenerative disorders: at a glance, Biomed. Pharmacother. 153 (2022 Sep 1) 113305, https://doi.org/10.1016/j.biopha.2022.113305.
- [37] P.B. Koli, K.H. Kapadnis, U.G. Deshpande, Transition metal decorated Ferrosoferric oxide (Fe3O4): an expeditious catalyst for photodegradation of Carbol Fuchsin in environmental remediation, J. Environ. Chem. Eng. 7 (5) (2019 Oct 1) 103373.
- [38] R.H. Waghchaure, V.A. Adole, B.S. Jagdale, P.B. Koli, Fe3+ modified zinc oxide nanomaterial as an efficient, multifaceted material for photocatalytic degradation of MB dye and ethanol gas sensor as part of environmental rectification, Inorg. Chem. Commun. 140 (2022 Jun 1) 109450.
- [39] P.B. Koli, S.G. Shinde, K.H. Kapadnis, A.P. Patil, M.P. Shinde, S.D. Khairnar, D.B. Sonawane, R.S. Ingale, Transition metal incorporated, modified bismuth oxide

- (Bi2O3) nano photo catalyst for deterioration of rosaniline hydrochloride dye as resource for environmental rehabilitation, J. Indian Chem. Soc. 98 (11) (2021 Nov 1) 10225
- [40] R.S. Shinde, V.A. Adole, S.D. Khairnar, P.B. Koli, T.B. Pawar, Study of Fe3O4 and Cu2+ doped modified Fe3O4 nano catalyst for photocatalytic degradation of methylene blue and eriochrome black-T dyes: synthesis, characterization, and antimicrobial assessment, Inorg. Chem. Commun. 170 (2024 Dec 1) 113206.
- [41] S.A. Ahire, A.A. Bachhav, B.S. Jagdale, A.V. Patil, P.B. Koli, T.B. Pawar, Amalgamation of ZrO2-PANI nanocomposite polymeric material: characterization and expeditious photocatalytic performance towards Carbol Fuchsin (CF) dye and kinetic study, J. Inorg. Organomet. Polym. Mater. 33 (5) (2023 May) 1357–1368.
- [42] R.S. Shinde, S.D. Khairnar, M.R. Patil, V.A. Adole, P.B. Koli, V.V. Deshmane, D.K. Halwar, R.A. Shinde, T.B. Pawar, B.S. Jagdale, A.V. Patil, Synthesis and characterization of ZnO/CuO nanocomposites as an effective photocatalyst and gas sensor for environmental remediation, J. Inorg. Organomet. Polym. Mater. 32 (3) (2022 Mar) 1045–1066.
- [43] S.A. Ahire, A.A. Bachhav, P.B. Koli, B.S. Jagdale, R.K. Pawar, T.B. Pawar, A.V. Patil, Polymeric Nanocomposite: Titania (TiO2)-Zirconia (ZrO2)-Polyaniline (PANI) for Sustainable Water Pollutant Removal, J. Indian Chem. Soc. (2025 May 14) 101762.
- [44] A. Klančnik, S. Piskernik, B. Jeršek, S.S. Možina, Evaluation of diffusion and dilution methods to determine the antibacterial activity of plant extracts, J. Microbiol. Methods 81 (2) (2010 May 1) 121–126, https://doi.org/10.1016/j.mimet.2010.02.004.
- [45] K.P. Suja, A. Jayalekshmy, C. Arumughan, Free radical scavenging behavior of antioxidant compounds of sesame (Sesamum indicum L.) in DPPH system, J. Agric. Food Chem. 52 (4) (2004 Feb 25) 912–915, https://doi.org/10.1021/ if0303621.
- [46] J. Yang, J. Ren, H. Guo, X. Qin, B. Han, J. Lin, Z. Li, The growth of Ni n clusters and their interaction with cubic, monoclinic, and tetragonal ZrO₂ surfaces—a theoretical and experimental study, RSCadvances 5 (74) (2015), https://doi.org/10.1039/ C5RA11706E.
- [47] Y. Sun, P. Zhang, B. Wang, J. Wu, S. Ning, A. Xie, Y. Shen, Hollow porous CuO/C nanorods as a high-performance anode for lithium ion batteries, J. Alloy. Compd. 750 (2018 Jun 25) 77–84, https://doi.org/10.1016/j.jallcom.2018.03.399.
- [48] A.M. Al-Mohaimeed, G.A. Mostafa, M.F. El-Tohamy, New construction of functionalized CuO/Al₂O₃ nanocomposite-based polymeric sensor for potentiometric estimation of naltrexone hydrochloride in commercial formulations, Polymers 13 (24) (2021 Dec 20) 4459, https://doi.org/10.3390/polym13244459.
- [49] A. Bentouami, M.S. Ouali, L.C. De Menorval, Photocatalytic decolourization of indigo carmine on 1, 10-phenanthrolinium intercalated bentonite under UV-B and solar irradiation, J. Photochem. Photobiol. A Chem. 212 (2-3) (2010 May 20) 101–106, https://doi.org/10.1016/j.jphotochem.2010.04.002.
- [50] C. Sánchez Trinidad, A. Martínez-De la Cruz, E. López Cuéllar, Photocatalytic degradation of indigo carmine by hydrothermally synthesized Bi₂MoO₆ in presence of EDTA, Environ. Sci. Pollut. Res. 22 (2) (2015 Jan) 792–799.
- [51] L. Lianmawii, N.M. Singh, Luminescence and photocatalytic degradation of indigo carmine in the presence of Sm³⁺ doped ZnS nanoparticles, Sci. Rep. 13 (1) (2023 Dec 17) 22450.
- [52] H.D. Wu, L.S. Chen, J.C. Hu, Photocatalytic degradation of indigo carmine by ZnO-Cu2O/graphene oxide composites synthesized via hydrothermal method, Adv. Mater. Res. 668 (2013 May 24) 105–109.
- [53] R.S. Ahmed, H.M. Hameed, M.W. Muayad, C.N. Salih, U.M. Nayef, A.A. Abed, A.M. Hussien, A. Awad, Photocatalytic degradation of indigo carmine by zinc oxide nanoparticles: effect of experimental parameters and kinetic degradation, Plasmonics (2025 Jun 7) 1–7.
- [54] N. Kermani, S.S. Mirzaee, M.E. Olya, S.M. Mirzaei, Synthesis, characterization and photocatalytic activity of CaZrO₃-SiO₂ nanocomposite for the decolorization of indigo carmine dye, Desalin. Water Treat. 125 (2018 Sep 1) 102–110, https://doi. org/10.5004/dwt.2018.23238.
- [55] D.N. Khanh, N.T. Tho, N.Q. Thang, N.T. Tien, C.T. Phong, M.Q. Cang, N.T. Phuong, Visible-light degradation of indigo carmine using a novel mixed metal oxides/reduced graphene oxide hybrid catalysts, Vietnam J. Sci. Technol. 57 (5) (2019 Oct 8) 572, https://doi.org/10.15625/2525-2518/57/5/13676.